Supplementary Information for Factors Governing H_3^+ Formation from Methyl Halogens and Pseudohalogens

Jacob Stamm[1], Swati S. Priyadarsini[1], Shawn Sandhu[1], Arnab Chakraborty[1], Jun Shen[1], Sung Kwon[1], Jesse Sandhu[1], Clayton Wicka[1], Arshad Mehmood[2,3], Benjamin G. Levine[2,3*], Piotr Piecuch[1,4*], Marcos Dantus[1,4*]

[1]Department of Chemistry, Michigan State University, East Lansing, 48824, Michigan, USA.
[2]Department of Chemistry, Stony Brook University, Stony Brook, 11794, New York, USA.
[3]Institute for Advanced Computational Science, Stony Brook University, Stony Brook, 11794, New York, USA.
[4]Department of Physics and Astronomy, Michigan State University, East Lansing, 48824, Michigan, USA.

*Corresponding author(s). E-mail(s): ben.levine@stonybrook.edu; piecuch@chemistry.msu.edu; dantus@chemistry.msu.edu;

1 Supplementary Data

1.1 Geometries of the CH_3X and CH_3X^{2+} species (X = OH, Cl, NCS, CN, SCN, I, and F)

In this section, we provide the Cartesian coordinates defining the geometries of the ground-state CH_3X molecules with X = OH, Cl, NCS, CN, SCN, I, and F obtained with CCSD and the low-lying states of the corresponding CH_3X^{2+} dications resulting from the DIP-EOMCC(3h-1p) (all systems) and DIP-EOMCC(4h-2p) (X = OH, Cl, and F) geometry optimizations carried out in the present study, along with the associated electronic energies. In the case of the CH_3Cl^{2+}, CH_3CN^{2+}, CH_3I^{2+}, and CH_3F^{2+} species that undergo Jahn-Teller distortion after vertical double ionization of their CH_3X parents, in addition to the information about low-lying singlet states, we provide the Cartesian coordinates and electronic energies of the minima on the lowest triplet potential surfaces. All Cartesian coordinates are in Å and all electronic energies are in Hartree (E_h). We also show the selected internuclear distances characterizing the low-lying electronic states of the CH_3X^{2+} dications with X = F, Cl, CN, and I and their CH_3X parents resulting from our most accurate CC and DIP-EOMCC computations to demonstrate that of all the calculated dicationic states, only the lowest singlets display the desired geometrical distortions that can lead to the liberation of a neutral H_2 which can subsequently roam the CHX^{2+} moiety to produce H_3^+ (see Supplementary Table 1).

CH_3OH

C_s-symmetric singlet ground state of CH_3OH ($X\,^1A'$)

CCSD/cc-pVDZ
(Energy = −115.412921 E_h)

	x	y	z
C	−0.7241393300	0.0123573000	0.0000000000
H	−1.1046333300	−1.0227208100	0.0000000000
H	−1.1260879000	0.5235695200	−0.8992260700
H	−1.1260879000	0.5235695200	0.8992260700
O	0.6910526200	−0.0639896600	0.0000000000
H	1.0163881800	0.8441714000	0.0000000000

CCSD/cc-pVTZ
(Energy = −115.536027 E_h)

	x	y	z
C	−0.7249886627	0.0127865238	0.0000000000
H	−1.0984167942	−1.0084579347	0.0000000000
H	−1.1121279840	0.5179968085	−0.8886032577
H	−1.1121279840	0.5179968085	0.8886032577
O	0.6888526485	−0.0639085990	0.0000000000
H	1.0300819364	0.8299326230	0.0000000000

Lowest $^1A'$ state of CH_3OH^{2+} (C_s)

DIP-EOMCC(3h-1p)/cc-pVDZ
(Energy = −114.364613 E_h)

	x	y	z
C	0.5928111302	−0.1114281951	0.0000000000
H	1.2371769027	−1.0268944634	0.0000000000
H	1.3083156417	1.0326902473	0.4396419447
H	1.3083156417	1.0326902473	−0.4396419447
O	−0.6125579732	−0.0320396337	0.0000000000
H	−1.1981889230	0.7973232577	0.0000000000

DIP-EOMCC(3h-1p)/cc-pVTZ
(Energy = −114.464806 E_h)

	x	y	z
C	−0.5887836762	0.1121232443	0.0000000000
H	−1.2260288660	1.0144855437	0.0000000000
H	−1.2987916719	−1.0278931681	0.4353821451
H	−1.2987916719	−1.0278931681	−0.4353821451
O	0.6064807080	0.0309179303	0.0000000000
H	1.2048022680	−0.7805426922	0.0000000000

DIP-EOMCC(4h-2p)/cc-pVDZ
(Energy = −114.379539 E_h)

	x	y	z
C	−0.5909140889	0.1196331147	0.0000000000
H	−1.2425133979	1.0374738324	0.0000000000
H	−1.3447174830	−1.0484731383	0.4355229179
H	−1.3447174830	−1.0484731383	−0.4355229179
O	0.6144321630	0.0278674099	0.0000000000
H	1.2101215198	−0.8017443103	0.0000000000

DIP-EOMCC(4h-2p)/cc-pVTZ
(Energy = −114.485619 E_h)

	x	y	z
C	−0.5811059989	0.1223595512	0.0000000000
H	−1.2283251026	1.0247199596	0.0000000000
H	−1.3162515641	−1.0406487206	0.4305954269
H	−1.3162515641	−1.0406487206	−0.4305954269
O	0.6161805298	0.0333686988	0.0000000000
H	1.2246407900	−0.7779530784	0.0000000000

CH_3Cl

C_{3v}-symmetric singlet ground state of CH_3Cl ($X\,^1A_1$)

CCSD/cc-pVDZ
(Energy = −499.439297 E_h)

	x	y	z
C	0.0000000000	0.0000000000	0.1847171661
H	−0.5205653991	0.9016457199	−0.1709999334
H	−0.5205653991	−0.9016457199	−0.1709999334
H	1.0411307983	0.0000000000	−0.1709999334
Cl	0.0000000000	0.0000000000	1.9695324050

CCSD/cc-pVTZ
(Energy = −499.553027 E_h)

	x	y	z
C	0.0000000000	0.0000000000	0.2073585681
H	−0.5139575119	0.8902005236	−0.1383064836
H	−0.5139575119	−0.8902005236	−0.1383064836
H	1.0279150238	0.0000000000	−0.1383064836
Cl	0.0000000000	0.0000000000	1.9892398828

Lowest $^1A'$ state of CH_3Cl^{2+} (C_s)

DIP-EOMCC(3h-1p)/cc-pVDZ
(Energy = −498.350224 E_h)

	x	y	z
C	0.2731539759	−0.1002996815	0.0000000000
H	1.2212283729	0.4881112307	0.0000000000
H	−0.7681794362	0.6326867718	0.4544508660
H	−0.7681794362	0.6326867718	−0.4544508660
Cl	0.0419665237	−1.6532550926	0.0000000000

DIP-EOMCC(3h-1p)/cc-pVTZ
(Energy = −498.445279 E_h)

	x	y	z
C	0.2722400000	−0.0937400000	0.0000000000
H	1.2075200000	0.4836600000	0.0000000000
H	−0.7591300000	0.6243900000	0.4504900000
H	−0.7591300000	0.6243900000	−0.4504900000
Cl	0.0383800000	−1.6386900000	0.0000000000

DIP-EOMCC(4h-2p)/cc-pVDZ
(Energy = −498.365933 E_h)

	x	y	z
C	0.2824800000	−0.1131500000	0.0000000000
H	1.2273300000	0.4894400000	0.0000000000
H	−0.7784700000	0.6452400000	−0.4494800000
H	−0.7784700000	0.6452400000	0.4494800000
Cl	0.0473900000	−1.6660300000	0.0000000000

DIP-EOMCC(4h-2p)/cc-pVTZ
(Energy = −498.467011 E_h)

	x	y	z
C	0.2808000000	−0.1038200000	0.0000000000
H	1.2140000000	0.4863100000	0.0000000000
H	−0.7681300000	0.6329500000	−0.4451600000
H	−0.7681300000	0.6329500000	0.4451600000
Cl	0.0410900000	−1.6487100000	0.0000000000

Lowest $^3A_2$ state of CH_3Cl^{2+} (C_{3v})

DIP-EOMCC(3h-1p)/cc-pVDZ
(Energy = −498.315487 E_h)

	x	y	z
C	0.0000000000	0.0000000000	0.2592943432
H	−0.5436762634	0.9416749112	−0.1726027421
H	−0.5436762634	−0.9416749112	−0.1726027421
H	1.0873525269	0.0000000000	−0.1726027421
Cl	0.0000000000	0.0000000000	1.8997637732

DIP-EOMCC(3h-1p)/cc-pVTZ
(Energy = −498.408020 E_h)

	x	y	z
C	0.0000000000	0.0000000000	0.2601474296
H	−0.5388484445	0.9333128835	−0.1695468059
H	−0.5388484445	−0.9333128835	−0.1695468059
H	1.0776968890	0.0000000000	−0.1695468059
Cl	0.0000000000	0.0000000000	1.8897428781

DIP-EOMCC(4h-2p)/cc-pVDZ
(Energy = −498.332407 E_h)

	x	y	z
C	0.0000000000	0.0000000000	0.2516157398
H	−0.5451005287	0.9441418110	−0.1710281014
H	−0.5451005287	−0.9441418110	−0.1710281014
H	1.0902010574	0.0000000000	−0.1710281014
Cl	0.0000000000	0.0000000000	1.9027184544

DIP-EOMCC(4h-2p)/cc-pVTZ
(Energy = −498.431670 E_h)

	x	y	z
C	0.0000000000	0.0000000000	0.2472082938
H	−0.5407748570	0.9366495277	−0.1651815292
H	−0.5407748570	−0.9366495277	−0.1651815292
H	1.0815497139	0.0000000000	−0.1651815292
Cl	0.0000000000	0.0000000000	1.8895861836

Lowest $^1A''$ state of CH_3Cl^{2+} (C_s)

DIP-EOMCC(3h-1p)/cc-pVDZ
(Energy = −498.291367 E_h)

	x	y	z
C	0.0993300000	0.0386900000	0.0000000000
H	1.1588100000	0.4408100000	0.0000000000
H	−0.6682600000	0.5852200000	0.7471400000
H	−0.6682600000	0.5852200000	−0.7471400000
Cl	0.0780200000	−1.6504200000	0.0000000000

DIP-EOMCC(3h-1p)/cc-pVTZ
(Energy = −498.385323 E_h)

	x	y	z
C	0.1007289189	0.0425763648	0.0000000000
H	1.1463924498	0.4387480844	0.0000000000
H	−0.6612410032	0.5786049986	0.7443063940
H	−0.6612410032	0.5786049986	−0.7443063940
Cl	0.0750006378	−1.6390144465	0.0000000000

DIP-EOMCC(4h-2p)/cc-pVDZ
(Energy = −498.306507 E_h)

	x	y	z
C	0.0980978909	0.0394779035	0.0000000000
H	1.1612351966	0.4446827881	0.0000000000
H	−0.6677027859	0.5843565468	0.7500648088
H	−0.6677027859	0.5843565468	−0.7500648088
Cl	0.0757124844	−1.6533537851	0.0000000000

DIP-EOMCC(4h-2p)/cc-pVTZ
(Energy = −498.406941 E_h)

	x	y	z
C	0.1013406288	0.0452612957	0.0000000000
H	1.1505838877	0.4432100889	0.0000000000
H	−0.6611890284	0.5752067193	0.7463936123
H	−0.6611890284	0.5752067193	−0.7463936123
Cl	0.0700935404	−1.6393648232	0.0000000000

CH_3NCS

C_1-symmetric singlet ground state of CH_3NCS ($X\,^1A$)

CCSD/cc-pVDZ
(Energy = −530.047090 E_h)

	x	y	z
C	−0.0430874086	1.4288667663	0.2952226821
H	−0.1624523251	1.4150226020	1.3923297041
H	0.8059905153	0.7862381561	0.0143879327
H	−0.9588142016	1.0331320467	−0.1767278587
N	0.2001287386	2.7717710939	−0.1679278989
C	−0.0594091995	3.9340281510	−0.0197748564
S	−0.3193840190	5.5056975739	0.0780191351

CCSD/cc-pVTZ
(Energy = −530.223212 E_h)

	x	y	z
C	−0.0533902880	1.4149846854	0.3022215603
H	−0.1595903548	1.3262356808	1.3821252049
H	0.8385541966	0.8805848315	−0.0156096905
H	−0.9213965466	0.9725272759	−0.1827740817
N	0.0544590415	2.7863046079	−0.0672222000
C	−0.0788248724	3.9536994985	−0.0070264695
S	−0.2168390762	5.5404198099	0.0038145164

Lowest $^1A'$ state of CH_3NCS^{2+} (C_s)

DIP-EOMCC(3h-1p)/cc-pVDZ
(Energy = −529.101569 E_h)

	x	y	z
C	−2.2235573634	0.3325447172	0.0000000000
H	−2.3897918795	1.4238551715	0.0000000000
H	−3.1981992623	−0.3297405693	0.4721124562
H	−3.1981992623	−0.3297405693	−0.4721124562
N	−1.1816216826	−0.4153637619	0.0000000000
C	0.0887776191	−0.0911201564	0.0000000000
S	1.5921472011	0.0669770482	0.0000000000

DIP-EOMCC(3h-1p)/cc-pVTZ
(Energy = −529.256416 E_h)

	x	y	z
C	2.2160730487	0.3196427654	0.0000000000
H	2.4074515357	1.3909230799	0.0000000000
H	3.1760876259	−0.3599693617	0.4613175767
H	3.1760876259	−0.3599693617	−0.4613175767
N	1.1681962028	−0.3919962850	0.0000000000
C	−0.0910982130	−0.0895719614	0.0000000000
S	−1.5818795560	0.0636370446	0.0000000000

CH_3CN

C_{3v}-symmetric singlet ground state of CH_3CN ($X\,^1A_1$)

CCSD/cc-pVDZ
(Energy = −132.383274 E_h)

	x	y	z
C	0.0000000000	0.0000000000	1.3077343117
H	−1.0363782120	0.0000000000	1.6820974597
H	0.5181891060	−0.8975298596	1.6820974597
H	0.5181891060	0.8975298596	1.6820974597
C	0.0000000000	0.0000000000	−0.1694291767
N	0.0000000000	0.0000000000	−1.3394634440

CCSD/cc-pVTZ
(Energy = −132.502749 E_h)

	x	y	z
C	0.0000000000	0.0000000000	1.2947644517
H	1.0230718530	0.0000000000	1.6639117025
H	−0.5115359265	−0.8860062146	1.6639117025
H	−0.5115359265	0.8860062146	1.6639117025
C	0.0000000000	0.0000000000	−0.1695509417
N	0.0000000000	0.0000000000	−1.3240504675

Lowest $^1A'$ state of CH_3CN^{2+} (C_s)

DIP-EOMCC(3h-1p)/cc-pVDZ
(Energy = −131.218826 E_h)

	x	y	z
C	1.2452770503	−0.0905299996	0.0000000000
H	1.8686511121	−1.0148994498	0.0000000000
H	1.8342358216	0.9583424369	0.4799615610
H	1.8342358216	0.9583424369	−0.4799615610
C	−0.1329953279	−0.0018989748	0.0000000000
N	−1.3524034478	0.0144146303	0.0000000000

DIP-EOMCC(3h-1p)/cc-pVTZ
(Energy = −131.318253 E_h)

	x	y	z
C	1.2324253057	−0.0899748074	0.0000000000
H	1.8517702020	−0.9977324518	0.0000000000
H	1.8125208609	0.9529362433	0.4745166072
H	1.8125208609	0.9529362433	−0.4745166072
C	−0.1323588435	−0.0060962988	0.0000000000
N	−1.3370655060	0.0170541414	0.0000000000

Lowest $^3A_2$ state of CH_3CN^{2+} (C_{3v})

DIP-EOMCC(3h-1p)/cc-pVDZ
(Energy = −131.192245 E_h)

	x	y	z
C	0.0000000000	0.0000000000	1.2642208984
H	−1.0798628536	0.0000000000	1.7217822694
H	0.5399314268	0.9351886638	1.7217822694
H	0.5399314268	−0.9351886638	1.7217822694
C	0.0000000000	0.0000000000	−0.0969200202
N	0.0000000000	0.0000000000	−1.3729762163

DIP-EOMCC(3h-1p)/cc-pVTZ
(Energy = −131.289462 E_h)

	x	y	z
C	0.0000000000	0.0000000000	−1.2502860282
H	1.0688043005	0.0000000000	−1.7102523500
H	−0.5344021503	0.9256116759	−1.7102523500
H	−0.5344021503	−0.9256116759	−1.7102523500
C	0.0000000000	0.0000000000	0.0962384495
N	0.0000000000	0.0000000000	1.3582621587

Lowest $^1A''$ state of CH_3CN^{2+} (C_s)

DIP-EOMCC(3h-1p)/cc-pVDZ
(Energy = −131.179926 E_h)

	x	y	z
C	1.2985026962	−0.0547533645	0.0000000000
H	1.7498132456	−1.0810794523	0.0000000000
H	1.8820612195	0.7781994086	0.6543094254
H	1.8820612195	0.7781994086	−0.6543094254
C	−0.1479606368	0.0027571296	0.0000000000
N	−1.3832230440	0.0099765501	0.0000000000

DIP-EOMCC(3h-1p)/cc-pVTZ
(Energy = −131.277823 E_h)

	x	y	z
C	1.2863374078	−0.0550263451	0.0000000000
H	1.7379065175	−1.0647142513	0.0000000000
H	1.8647150066	0.7772767936	0.6445018403
H	1.8647150066	0.7772767936	−0.6445018403
C	−0.1481071690	0.0032045274	0.0000000000
N	−1.3695922594	0.0098079517	0.0000000000

CH_3SCN

C_s-symmetric singlet ground state of CH_3SCN ($X\,^1A'$)

CCSD/cc-pVDZ
(Energy = −530.045875 E_h)

	x	y	z
C	−1.4873446166	0.9564956407	0.0000000000
H	−2.5571166809	0.6897211407	0.0000000000
H	−1.2515248885	1.5363117028	−0.9056542676
H	−1.2515248885	1.5363117028	0.9056542676
S	−0.5877877070	−0.6311421874	0.0000000000
C	1.0114490965	−0.0195553661	0.0000000000
N	2.1191915149	0.3710976765	0.0000000000

CCSD/cc-pVTZ
(Energy = −530.220758 E_h)

	x	y	z
C	−1.4773763038	0.9522270837	0.0000000000
H	−2.5326888992	0.6885620658	0.0000000000
H	−1.2416694918	1.5205833083	−0.8941829079
H	−1.2416694918	1.5205833083	0.8941829079
S	−0.5810473992	−0.6287148113	0.0000000000
C	1.0057326023	−0.0204045848	0.0000000000
N	2.0967352535	0.3725494800	0.0000000000

Lowest $^1A'$ state of CH_3SCN^{2+} (C_s)

DIP-EOMCC(3h-1p)/cc-pVDZ
(Energy = −529.031498 E_h)

	x	y	z
C	1.5871308858	−0.8141213706	0.0000000000
H	1.1232827739	−1.8147634893	0.0000000000
H	2.3332500048	−0.6104440229	−0.8454390975
H	2.3332500048	−0.6104440229	0.8454390975
S	0.5461868141	0.5603585618	0.0000000000
C	−0.9999281560	−0.0417634976	0.0000000000
N	−2.1704137573	−0.3313139186	0.0000000000

DIP-EOMCC(3h-1p)/cc-pVTZ
(Energy = −529.187449 E_h)

	x	y	z
C	−1.5709464732	−0.8108416597	0.0000000000
H	−1.1164935506	−1.7987881482	0.0000000000
H	−2.3164864580	−0.6039512318	−0.8320721415
H	−2.3164864580	−0.6039512318	0.8320721415
S	−0.5416090935	0.5555750472	0.0000000000
C	0.9968727289	−0.0322518808	0.0000000000
N	2.1489629545	−0.3336937848	0.0000000000

CH_3I

C_{3v}-symmetric singlet ground state of CH_3I (X^1A_1)

CCSD/cc-pVTZ (cc-pVTZ-PP for I)
(Energy = −334.703744 E_h)

	x	y	z
C	0.0000000000	0.0000000000	−0.0393656028
H	0.5153338175	−0.8925843548	−0.3725932276
H	0.5153338175	0.8925843548	−0.3725932276
H	−1.0306676350	0.0000000000	−0.3725932276
I	0.0000000000	0.0000000000	2.0954312732

Lowest $^3A_2$ state of CH_3I^{2+} (C_{3v})

DIP-EOMCC(3h-1p)/cc-pVTZ (cc-pVTZ-PP for I)
(Energy = −333.718094 E_h)

	x	y	z
C	0.0000000000	0.0000000000	−0.0803511236
H	0.5329063175	−0.9230208177	−0.3443115166
H	0.5329063176	0.9230208177	−0.3443115166
H	−1.0658126351	0.0000000000	−0.3443115166
I	0.0000000000	0.0000000000	2.0514173811

Lowest $^1A'$ state of CH_3I^{2+} (C_s)

DIP-EOMCC(3h-1p)/cc-pVTZ (cc-pVTZ-PP for I)
(Energy = −333.681921 E_h)

	x	y	z
C	−0.0025023416	−0.0468605810	0.0000000000
H	−1.0653514747	−0.3528160991	0.0000000000
H	0.5321081138	−0.3480335091	0.9219109922
H	0.5321081138	−0.3480335091	−0.9219109922
I	0.0030554118	2.0312802676	0.0000000000

Lowest $^1A''$ state of CH_3I^{2+} (C_s)

DIP-EOMCC(3h-1p)/cc-pVTZ (cc-pVTZ-PP for I)
(Energy = −333.681917 E_h)

	x	y	z
C	0.0007606003	−0.0463309967	0.0000000000
H	−1.0641584109	−0.3490174572	0.0000000000
H	0.5317725817	−0.3491721414	0.9225167771
H	0.5317725817	−0.3491721414	−0.9225167771
I	−0.0002741251	2.0319055728	0.0000000000

CH_3F

C_{3v}-symmetric singlet ground state of CH_3F (X^1A_1)

CCSD/cc-pVDZ
(Energy = −139.400993 E_h)

	x	y	z
C	0.0000000000	0.0000000000	−0.1109762154
H	−0.5205661753	0.9016470643	−0.4791719638
H	−0.5205661753	−0.9016470643	−0.4791719638
H	1.0411323506	0.0000000000	−0.4791719638
F	0.0000000000	0.0000000000	1.2717739596

CCSD/cc-pVTZ
(Energy = −139.544752 E_h)

	x	y	z
C	0.0000000000	0.0000000000	−0.1163991213
H	−0.5141911648	0.8906052223	−0.4736553424
H	−0.5141911648	−0.8906052223	−0.4736553424
H	1.0283823297	0.0000000000	−0.4736553424
F	0.0000000000	0.0000000000	1.2603625185

Lowest $^1A'$ state of CH_3F^{2+} (C_s)

DIP-EOMCC(3h-1p)/cc-pVDZ
(Energy = −138.241236 E_h)

	x	y	z
C	−0.5985953800	−0.1368574900	0.0000000000
H	−1.2120732100	−1.0896275000	0.0000000000
H	−1.2744019000	1.0446947800	0.4504430900
H	−1.2744019000	1.0446947800	−0.4504430900
F	0.5779066100	0.0334895200	0.0000000000

DIP-EOMCC(3h-1p)/cc-pVTZ
(Energy = −138.363507 E_h)

	x	y	z
C	−0.5952859869	−0.1381623787	0.0000000000
H	−1.1957834119	−1.0829979638	0.0000000000
H	−1.2749641033	1.0350869558	−0.4477669751
H	−1.2749641033	1.0350869558	0.4477669751
F	0.5732561154	0.0352157610	0.0000000000

DIP-EOMCC(4h-2p)/cc-pVDZ
(Energy = −138.255656 E_h)

	x	y	z
C	−0.5876170848	−0.1483935076	0.0000000000
H	−1.2136392476	−1.1020827596	0.0000000000
H	−1.2851716442	1.0602657448	0.4484010374
H	−1.2851716442	1.0602657448	−0.4484010374
F	0.5900338409	0.0263387575	0.0000000000

DIP-EOMCC(4h-2p)/cc-pVTZ
(Energy = −138.383500 E_h)

	x	y	z
C	0.5939614495	0.1439448346	0.0000000000
H	1.2061452639	1.0903840225	0.0000000000
H	1.2934773458	−1.0546282113	−0.4444578329
H	1.2934773458	−1.0546282113	0.4444578329
F	−0.5759298050	−0.0369457945	0.0000000000

Lowest $^3A_2$ state of CH_3F^{2+} (C_{3v})

DIP-EOMCC(3h-1p)/cc-pVDZ
(Energy = −138.148440 E_h)

	x	y	z
C	0.0000000000	0.0000000000	0.0361587218
H	−0.5743605946	0.9948217317	−0.5246893880
H	−0.5743605946	−0.9948217317	−0.5246893880
H	1.1487211892	0.0000000000	−0.5246893880
F	0.0000000000	0.0000000000	1.2612726858

DIP-EOMCC(3h-1p)/cc-pVTZ
(Energy = −138.269307 E_h)

	x	y	z
C	0.0000000000	0.0000000000	0.0453185087
H	−0.5717237553	0.9902545921	−0.5274179368
H	−0.5717237553	−0.9902545921	−0.5274179368
H	1.1434475106	0.0000000000	−0.5274179368
F	0.0000000000	0.0000000000	1.2598128767

DIP-EOMCC(4h-2p)/cc-pVDZ
(Energy = −138.162329 E_h)

	x	y	z
C	0.0000000000	0.0000000000	−0.6146661484
H	−0.5747031714	0.9954150921	−1.1734457355
H	−0.5747031714	−0.9954150921	−1.1734457355
H	1.1494063428	0.0000000000	−1.1734457355
F	0.0000000000	0.0000000000	0.6146661484

DIP-EOMCC(4h-2p)/cc-pVTZ
(Energy = −138.289244 E_h)

	x	y	z
C	0.0000000000	0.0000000000	−0.6105540550
H	−0.5713222489	0.9895591625	−1.1741748611
H	−0.5713222489	−0.9895591625	−1.1741748611
H	1.1426444978	0.0000000000	−1.1741748611
F	0.0000000000	0.0000000000	0.6104124310

Lowest $^1A''$ state of CH_3F^{2+} (C_s)[†]

DIP-EOMCC(3h-1p)/cc-pVDZ
(Energy = −138.121049 E_h)

	x	y	z
C	−0.1178970430	−0.0000588735	0.0411263924
H	−0.6110998016	0.9612951465	−0.5361534533
H	−0.6101248101	−0.9616750927	−0.5359042126
H	1.2735740657	0.0000858601	−0.5047819781
F	0.0655475889	0.0003529596	1.2589951043

[†]We experienced numerical difficulties in converging the geometry of the lowest $^1A''$ state of CH_3F^{2+} when the DIP-EOMCC(4h-2p) approach using the cc-pVDZ and cc-pVTZ basis sets and the DIP-EOMCC(3h-1p) method using the cc-pVTZ basis were employed. We were able to locate the equilibrium geometry of the lowest $^1A''$ state of CH_3F^{2+} at the DIP-EOMCC(3h-1p)/cc-pVDZ theory level, but again encountered numerical difficulties when attempting to locate the minimum using its true C_s symmetry. Therefore, we only report the Cartesian coordinates that were obtained without imposing any symmetry constraints during the search for the relevant minimum. As in all other geometry optimizations carried out in the present study, the search for the minimum on the lowest $^1A''$ potential was stopped when the absolute value of the largest component of the energy gradient became smaller than 0.0001 E_h/a_0 and the root-mean-square gradient fell below one-third of that value (default geometry optimization convergence criteria in GAMESS).

Supplementary Table 1: Comparison of the selected internuclear distances, in Å, characterizing the low-lying electronic states of the doubly ionized CH_3X molecules with X = F, Cl, CN, and I, which are most relevant to H_3^+ formation, with their counterparts in the ground-state neutral CH_3X species. The equilibrium geometries of the CH_3X molecules were determined with CCSD, whereas those characterizing the CH_3X^{2+} dications were obtained using the DIP-EOMCC(4h-2p) (X = F and Cl) and DIP-EOMCC(3h-1p) (X = F, CN, and I) approaches. The calculations for the X = Cl, CN, and I species employed the cc-pVTZ basis set (with an additional tight d function for a chlorine atom and using the cc-pVTZ-PP basis for iodine). In the case of the neutral and doubly ionized CH_3F molecules, where we experienced difficulties in converging the geometry of the lowest $^1A''(C_s)$ state of CH_3F^{2+} when the DIP-EOMCC(4h-2p) method using the cc-pVDZ and cc-pVTZ basis sets and the DIP-EOMCC(3h-1p) approach using cc-pVTZ were employed, we provide the CCSD/cc-pVDZ and DIP-EOMCC(3h-1p)/cc-pVDZ data, showing the results of the CCSD/cc-pVTZ calculations for CH_3F and the DIP-EOMCC(4h-2p)/cc-pVTZ computations for the $^1A'(C_s)$ and $^3A_2(C_{3v})$ states of CH_3F^{2+} in parentheses (cf. the footnote on Page 11).

X = F					X = Cl				
Bond	Neutral	Dication			Bond	Neutral	Dication		
	$^1A_1(C_{3v})$	$^1A'(C_s)$	$^3A_2(C_{3v})$	$^1A''(C_s)$		$^1A_1(C_{3v})$	$^1A'(C_s)$	$^3A_2(C_{3v})$	$^1A''(C_s)$
C–H(1)	1.104 (1.089)	1.133 (1.127)	1.278 (1.274)	1.495	C–H(1)	1.084	1.104	1.158	1.122
C–H(2)	1.104 (1.089)	1.434 (1.457)	1.278 (1.274)	1.225	C–H(2)	1.084	1.357	1.158	1.191
C–H(3)	1.104 (1.089)	1.434 (1.457)	1.278 (1.274)	1.225	C–H(3)	1.084	1.357	1.158	1.191
H(2)–H(3)	1.803 (1.781)	0.901 (0.889)	1.990 (1.979)	1.923	H(2)–H(3)	1.780	0.890	1.873	1.493
X = CN					X = I				
Bond	Neutral	Dication			Bond	Neutral	Dication		
	$^1A_1(C_{3v})$	$^1A'(C_s)$	$^3A_2(C_{3v})$	$^1A''(C_s)$		$^1A_1(C_{3v})$	$^1A'(C_s)$	$^3A_2(C_{3v})$	$^1A''(C_s)$
C–H(1)	1.088	1.099	1.164	1.106	C–H(1)	1.083	1.106	1.098	1.107
C–H(2)	1.088	1.284	1.164	1.201	C–H(2)	1.083	1.107	1.098	1.107
C–H(3)	1.088	1.284	1.164	1.201	C–H(3)	1.083	1.107	1.098	1.107
H(2)–H(3)	1.772	0.949	1.851	1.289	H(2)–H(3)	1.785	1.844	1.846	1.845

1.2 DIP-EOMCC results that were used to calibrate CASSCF-based AIMD simulations and information about the neutral and doubly ionized CH_3F species

The purpose of this section is to show representative results of the DIP-EOMCC computations that were used to calibrate our CASSCF-based AIMD simulations for the CH_3OH^{2+}, CH_3Cl^{2+}, CH_3CN^{2+}, CH_3SCN^{2+}, and CH_3F^{2+} dications (Supplementary Figs. 1 and 2) and to summarize our most accurate CC/DIP-EOMCC calculations for the doubly ionized and neutral CH_3F species relevant to the analysis of the applicability of conditions (i)–(iii) in the Discussion section of the main text to CH_3F^{2+} (Supplementary Fig. 3 and Supplementary Table 2). Supplementary Fig. 1 provides information about the vertical and adiabatic double ionization energies of the CH_3X molecules with X = F, OH, Cl, CN, and SCN associated with the lowest singlet (all systems) and triplet (X = F, Cl, and CN) states of the respective dications and the resulting adiabatic relaxation energies $\Delta E_{\rm rlx}$, defined by Eq. (1) of the main text, obtained in the DIP-EOMCC/cc-pVDZ calculations, which are subsequently compared, along with the H(2)–H(3) distances characterizing the CH_3F^{2+}, CH_3OH^{2+}, CH_3Cl^{2+}, CH_3CN^{2+}, and CH_3SCN^{2+} dications, with their CAS(4,4)SCF/cc-pVDZ counterparts in Supplementary Fig. 2. Supplementary Fig. 3, which is an extended version of the main text's Fig. 6 augmented with the CH_3F^{2+} data, shows the H(2)–H(3) distances and the adiabatic relaxation and dissociation energies, $\Delta E_{\rm rlx}$ and $\Delta E_{\rm diss}$, respectively, defined in the main text by Eqs. (1) and (2), that characterize the lowest singlet states of the doubly ionized CH_3X molecules with X = F, OH, Cl, NCS, CN, SCN, and I obtained in the most accurate DIP-EOMCC computations carried out in the present study, alongside the normalized yields of H_3^+ relative to all dication channels taken from Table 1 of the main text for X = OD, Cl, and NCS and assumed to by zero for the remaining species that do not generate appreciable H_3^+ amounts. The companion Supplementary Table 2 reports the selected internuclear distances characterizing the doubly ionized CH_3F molecule in its lowest singlet state, which are most relevant to H_3^+ formation in the roaming mechanism considered in the present study, and their counterparts characterizing the ground-state CH_3F species, along with the vertical and adiabatic double ionization energies, $\Delta E_{\rm vert}$ and $\Delta E_{\rm adiab}$, respectively, and the $\Delta E_{\rm rlx}$ and $\Delta E_{\rm diss}$ values associated with the CH_3F^{2+} dication, again resulting from the most accurate CC/DIP-EOMCC calculations carried out in this work. For further details of these calculations, see the captions to Supplementary Fig. 3 and Supplementary Table 2.

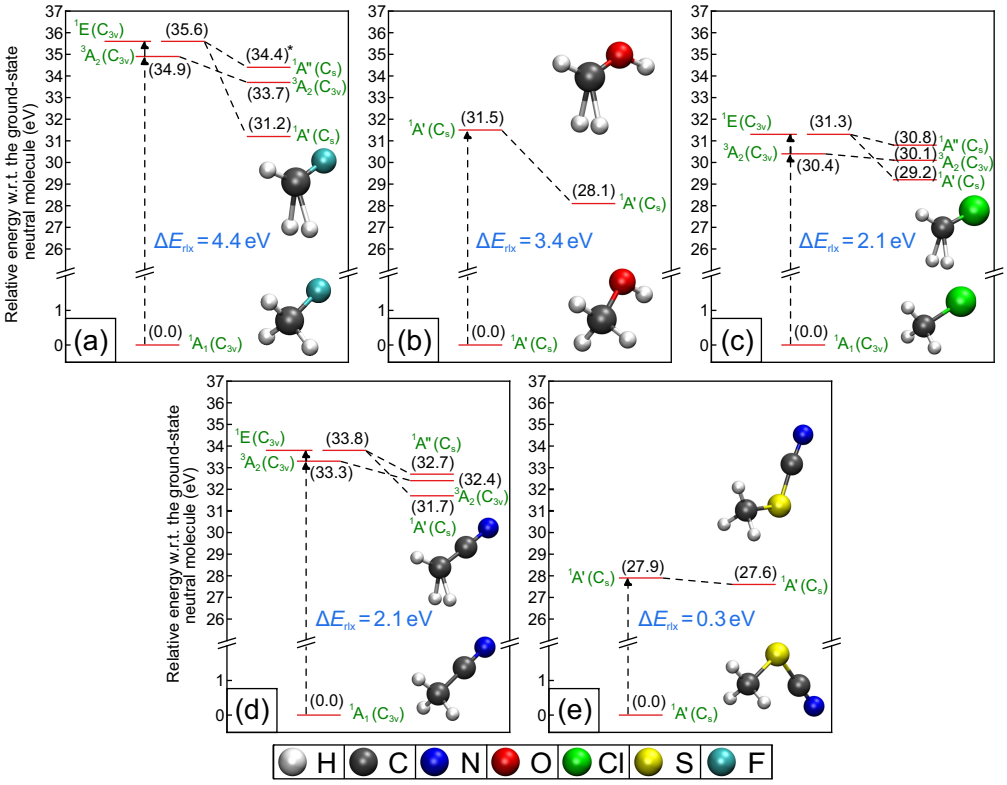

Supplementary Fig. 1: Energy level diagrams and molecular geometries associated with the double ionization of CH_3X species. The vertical and adiabatic double ionization energies, in eV, of (a) CH_3F, (b) CH_3OH, (c) CH_3Cl, (d) CH_3CN, and (e) CH_3SCN molecules associated with the lowest singlet (all systems) and triplet (CH_3F, CH_3Cl, and CH_3CN) states of the respective dications resulting from the DIP-EOMCC(4h-2p) (CH_3F, CH_3OH, and CH_3Cl) and DIP-EOMCC(3h-1p) (the remaining species) computations are shown. The cc-pVDZ basis set (with an additional tight d function for each of S and Cl atoms) was employed throughout and all double ionization energies are reported relative to the respective CH_3X ground states obtained in the CCSD/cc-pVDZ calculations. In each panel, the multiplicities, irreducible representations, and point group symmetries of the states of interest are highlighted in green and the adiabatic relaxation energies $\Delta E_{\rm rlx}$, obtained by subtracting the adiabatic double ionization energies from their vertical counterparts corresponding to the lowest singlet states of the CH_3X^{2+} dications (see Eq. (1) in the main text), are emphasized using blue font. Because of the numerical difficulties with locating the minimum on the lowest $^1A''$ potential of the CH_3F^{2+} dication using the DIP-EOMCC(4h-2p) approach, explained in the footnote on page 11, the adiabatic double ionization energy corresponding to this minimum, marked in panel (a) by the asterisk, is a value resulting from the DIP-EOMCC(3h-1p)/cc-pVDZ calculations (34.8 eV) lowered by the effect of replacing DIP-EOMCC(3h-1p) by DIP-EOMCC(4h-2p) which, based on the results obtained for the remaining states of CH_3F^{2+} considered in this work, is estimated at 0.4 eV. All data used to create the figure are included within it.

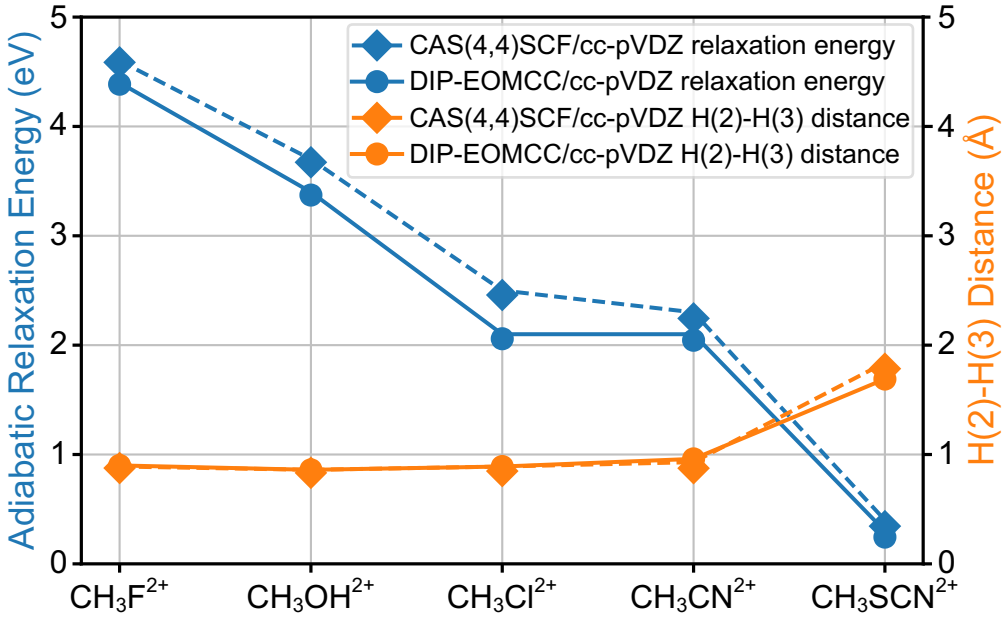

Supplementary Fig. 2: Calibration of the CASSCF approach to the DIP-EOMCC data. Compared are the adiabatic relaxation energies $\Delta E_{\rm rlx}$, in eV, defined by Eq. (1) in the main text, characterizing the lowest singlet states of the CH_3X^{2+} dications with X = F, OH, Cl, CN, and SCN (blue lines and symbols) and the H(2)–H(3) distances, in Å, in the same species (orange lines and symbols) obtained using the CAS(4,4)SCF/cc-pVDZ approach (dashed lines and diamonds) with the corresponding DIP-EOMCC/cc-pVDZ data (solid lines and circles). In the case of the latter calculations, the CH_3F^{2+}, CH_3OH^{2+}, and CH_3Cl^{2+} species were handled with DIP-EOMCC(4h-2p) and we used DIP-EOMCC(3h-1p) for CH_3CN^{2+} and CH_3SCN^{2+}. All data are included in the Source Data folder.

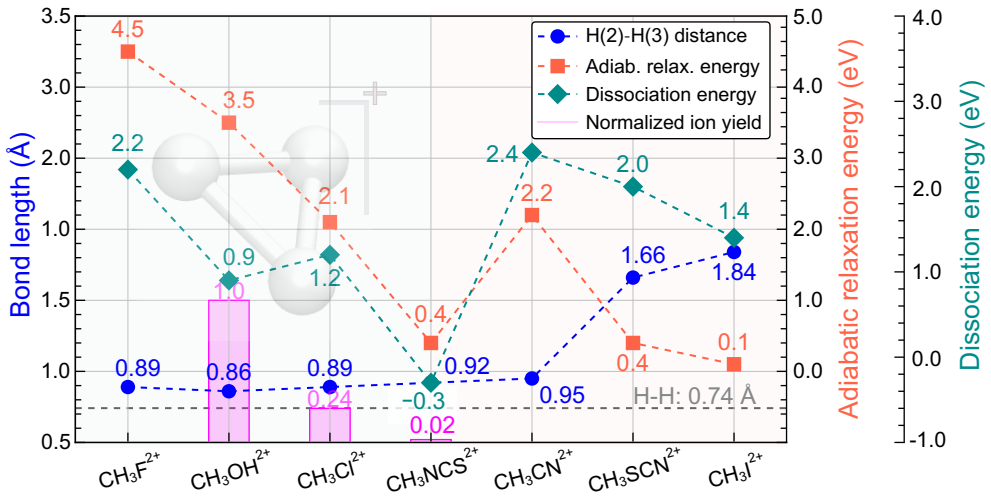

Supplementary Fig. 3: Comparison of the parameters that are most relevant to explaining the trends in H_3^+ yields. The H(2)–H(3) distances, in Å, in the CH_3X^{2+} dications, where X = F, OH, Cl, NCS, CN, SCN, and I (blue numbers, circles, and line), the adiabatic relaxation energies $\Delta E_{\rm rlx}$ (Eq. (1) in the main text), in eV, corresponding to the lowest singlet states of the doubly ionized CH_3X molecules (red numbers, squares, and line), and the dissociation energies $\Delta E_{\rm diss}$ (Eq. (2) in the main text), also in eV, associated with the fragmentation of the CH_3X^{2+} species into H_2 and CHX^{2+} (green numbers, diamonds, and line) resulting from the most accurate DIP-EOMCC computations carried out in the present study are shown alongside the normalized yields of H_3^+ relative to all dication channels taken from Table 1 of the main text for X = OD, Cl, and NCS (magenta numbers and bars) and assumed to be zero for the remaining species that do not generate appreciable H_3^+ amounts. The H(2)–H(3) distances and the adiabatic relaxation energies $\Delta E_{\rm rlx}$ were computed using the DIP-EOMCC(4h-2p)/cc-pVTZ theory level for X = F, OH, and Cl and DIP-EOMCC(3h-1p)/cc-pVTZ (cc-pVTZ-PP for I atom) for the remaining CH_3X^{2+} dications. The dissociation energies $\Delta E_{\rm diss}$ were determined using the DIP-EOMCC(3h-1p) approach for CH_3X^{2+} and CHX^{2+} and CCSD for H_2. In this case, the calculations of the $\Delta E_{\rm diss}$ values characterizing the doubly ionized CH_3X species with X = F, OH, Cl, NCS, CN, and SCN used the cc-pVDZ basis set. The $\Delta E_{\rm diss}$ calculations for CH_3I^{2+} relied on the cc-pVTZ basis for C and H atoms and cc-pVTZ-PP for iodine. As mentioned in the Methods: Electronic structure calculations section of the main text, the cc-pVDZ and cc-pVTZ basis sets adopted in this work contain additional tight d functions for S and Cl atoms. The H–H bond length of an isolated H_2 molecule is highlighted in gray. All data used to create the figure are included within it.

Supplementary Table 2: Comparison of the selected internuclear distances, in Å, characterizing the doubly ionized CH_3F molecule in its lowest singlet state, which are most relevant to H_3^+ formation, with their counterparts in the neutral CH_3F species, along with the corresponding vertical and adiabatic double ionization energies, ΔE_{vert} and $\Delta E_{\mathrm{adiab}}$, respectively, the adiabatic relaxation energy ΔE_{rlx}, and the dissociation energy ΔE_{diss}, in eV, associated with the CH_3F^{2+} dication (for the definitions of ΔE_{rlx} and ΔE_{diss}, see Eqs. (1) and (2) in the main text). The equilibrium geometry and energetics of the CH_3F molecule were computed with the CCSD/cc-pVTZ approach, whereas the structural parameters of the doubly ionized CH_3F in its lowest singlet state relevant to H_3^+ formation and the associated ΔE_{vert}, $\Delta E_{\mathrm{adiab}}$, and ΔE_{rlx} values were determined using the DIP-EOMCC(4h-2p)/cc-pVTZ approach. The geometries and energies of the CH_3F^{2+} and CHF^{2+} species in their lowest singlet states entering the definition of ΔE_{diss} were obtained at the DIP-EOMCC(3h-1p)/cc-pVDZ theory level. The analogous information characterizing the neutral H_2 molecule, needed to determine ΔE_{diss} as well, was obtained in the CCSD/cc-pVDZ calculations.

Bond length				
Bond	Neutral	Dication	Energy type	
C–H(1)	1.089	1.127	ΔE_{vert}	36.1
C–H(2)	1.089	1.457	$\Delta E_{\mathrm{adiab}}$	31.6
C–H(3)	1.089	1.457	ΔE_{rlx}	4.5
H(2)–H(3)	1.781	0.889	ΔE_{diss}	2.2

2 Supplementary Discussion

2.1 Potential energy profiles for the $CH_3X^{2+} \rightarrow CX^+ + H_3^+$ reactions (X = OH, Cl, and NCS)

This section provides information about the potential energy profiles for the $CH_3X^{2+} \rightarrow CX^+ + H_3^+$ reactions initiated by double ionization of the CH_3X molecules with X = OH, Cl, and NCS obtained in our CC/DIP-EOMCC computations. The main goal of these computations was to identify structures that define barriers to H_3^+ formation and to demonstrate that the CH_3OH^{2+}, CH_3Cl^{2+}, and CH_3NCS^{2+} dications created in our double ionization experiments have enough energy not only to overcome the relevant barriers, but also to liberate the neutral H_2 molecule, which is a crucial step for the roaming mechanism explored in our study.

As explained in the main text, there are two key events that must take place for a CH_3X^{2+} dication to form H_3^+: the dissociation of a neutral H_2 from the doubly ionized CH_3X species and the proton abstraction from the remaining CHX^{2+} moiety by the roaming H_2 molecule. As shown by Matsubara, who examined the CH_3X^{2+} systems with X = F, Cl, and Br in Ref. [1], and as confirmed by our DIP-EOMCC calculations for the CH_3OH^{2+}, CH_3Cl^{2+}, and CH_3NCS^{2+} dications that form H_3^+ in our experiments, the liberation of a neutral H_2 from its doubly ionized CH_3X parent is an energetically uphill barrierless process, i.e., there are no intervening transition states between the minima on the lowest singlet potential energy surfaces of the CH_3X^{2+} species and the respective $CH_3X^{2+} \rightarrow CHX^{2+} + H_2$ dissociation asymptotes. There are, however, transition states that connect the equilibrium CH_3X^{2+} structures to the final H_3^+ and CX^+ products, which are associated with the abstraction of a proton from the CHX^{2+} fragment by the roaming H_2. This is illustrated in Supplementary Fig. 4, where we show the minimum energy paths for the formation of H_3^+ from the CH_3X^{2+} dications resulting from double ionization of the CH_3X molecules with X = OH, Cl, and NCS, after these dications relax to their respective equilibrium geometries, along with the corresponding $CH_3X^{2+} \rightarrow CHX^{2+} + H_2$ dissociation asymptotes, obtained in the DIP-EOMCC(3h-1p)/cc-pVDZ computations for the CH_3X^{2+}, CHX^{2+}, and CX^+ species and using CCSD/cc-pVDZ for CH_3X, H_2, and H_3^+. In the case of the doubly ionized CH_3OH^{2+} and CH_3Cl^{2+} compounds, shown in Supplementary Fig. 4 in panels (a) and (b), respectively, we see the presence of a saddle point that corresponds to a particular edge-on configuration between the H_2 molecule and the $CHOH^{2+}$ and $CHCl^{2+}$ moieties, which facilitates the completion of the final proton abstraction step $CHX^{2+} + H_2 \rightarrow CX^+ + H_3^+$ of the $CH_3X^{2+} \rightarrow CX^+ + H_3^+$ process. As shown in Supplementary Fig. 4 (c), when the CH_3NCS^{2+} system is examined, the reaction profile connecting the CH_3NCS^{2+} dication minimum with the $CNCS^+ + H_3^+$ products, which features two saddle points and an intermediate structure between them, is somewhat more complicated, since the NCS functional group consists of three atoms, but the overall picture is similar. The second (and final) transition state and the intermediate structure located immediately before it, which is a complex formed by H_2 and the $CHNCS^{2+}$ moiety, form favorable edge-on configurations between the H_2 and $CHNCS^{2+}$ species that enable the $CHNCS^{2+} + H_2 \rightarrow CNCS^+ + H_3^+$ proton abstraction step needed to complete the $CH_3NCS^{2+} \rightarrow CNCS^+ + H_3^+$ process. In this case,

the CH_3NCS^{2+} dication, after relaxing to the minimum on its lowest singlet potential, can either directly dissociate to produce a neutral H_2 or overcome the first barrier characterizing the highest-energy transition state on the energy profile shown in panel (c) of Supplementary Fig. 4 to land on the relatively flat part of the potential surface, where it can liberate a neutral H_2, start the roaming process, and surpass the second barrier corresponding to the transition state connecting the aforementioned complex formed by H_2 and $CHNCS^{2+}$ with the H_3^+ and $CNCS^+$ reaction products. Irrespective of the above differences between the potential energy profiles describing the $CH_3OH^{2+} \rightarrow COH^+ + H_3^+$ and $CH_3Cl^{2+} \rightarrow CCl^+ + H_3^+$ processes and the $CH_3NCS^{2+} \rightarrow CNCS^+ + H_3^+$ reaction pathway, the adiabatic relaxation energies $\Delta E_{\rm rlx}$ characterizing the CH_3X^{2+} dications with X = OH, Cl, and NCS are sufficiently large to overcome the barriers associated with the transition states on their respective lowest singlet potentials and liberate neutral H_2 molecules that can subsequently roam their CHX^{2+} companions, abstracting protons from them to form H_3^+. This means that the CH_3X^{2+} species with X = OH, Cl, and NCS meet the energetic condition (iii) laid down in the Discussion section of the main text in its entirety, in addition to satifying the geometrical criteria (i) and (ii). In the context of the above analysis, it is also worth pointing out that the geometries and energies of the stationary points along the $CH_3OH^{2+} \rightarrow COH^+ + H_3^+$ and $CH_3Cl^{2+} \rightarrow CCl^+ + H_3^+$ reaction pathways obtained in our DIP-EOMCC computations, including the transition states and the associated barrier heights relative to the respective CH_3X^{2+} dication minima, are in good agreement with their counterparts reported in Ref. [2] for CH_3OH^{2+} and Ref. [1] for CH_3Cl^{2+}. This strengthens the validity of our computations and conclusions drawn from them.

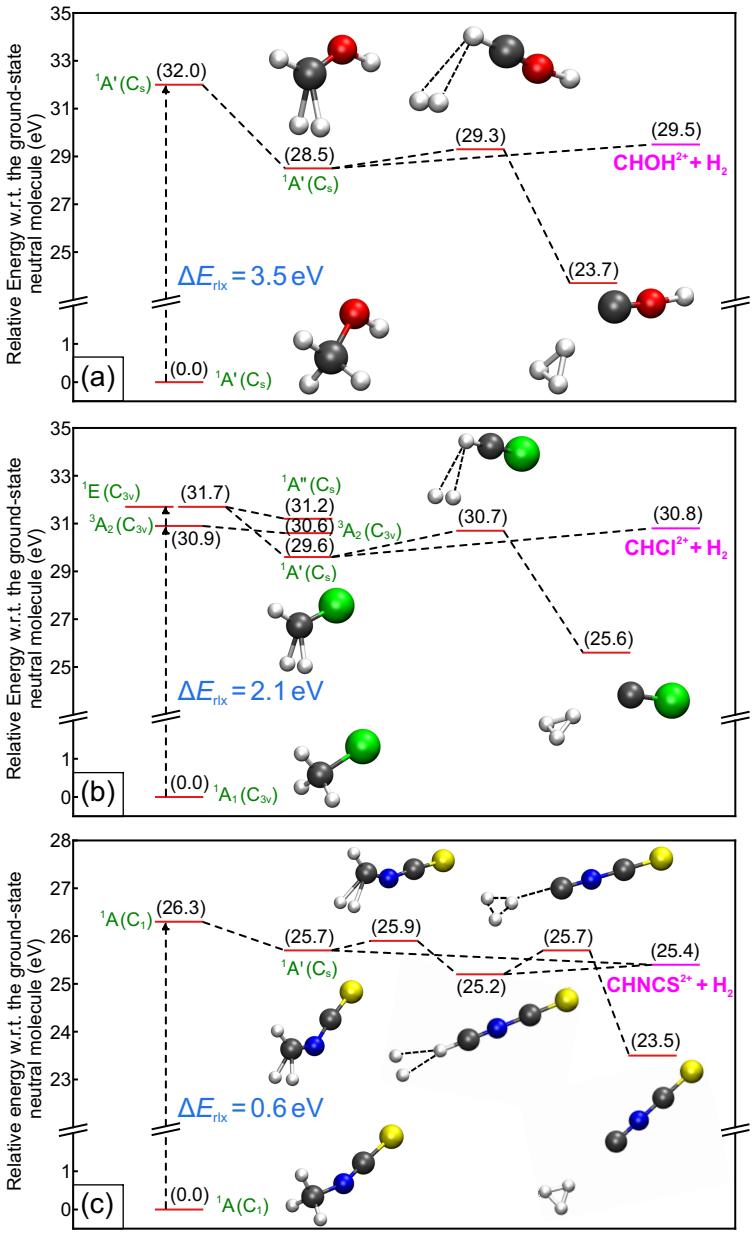

Supplementary Fig. 4: Potential energy profiles for H_3^+ formation from doubly ionized CH_3X species. The energy profiles (in eV) illustrate the $CH_3X^{2+} \rightarrow CX^+ + H_3^+$ reactions following double ionization of the CH_3X molecules with (a) X = OH, (b) X = Cl, and (c) X = NCS, along with the corresponding $CH_3X^{2+} \rightarrow CHX^{2+} + H_2$ dissociation asymptotes relevant to the roaming mechanism examined in the present

study, obtained with the DIP-EOMCC(3h-1p) approach for the CH_3X^{2+}, CHX^{2+}, and CX^+ species and CCSD for CH_3X, H_2, and H_3^+. The cc-pVDZ basis set (with an additional tight d function for each of S and Cl atoms) was employed throughout and all energies are reported relative to the respective CH_3X ground states resulting from the CCSD/cc-pVDZ computations. The multiplicities, irreducible representations, and point group symmetries of the electronic states of interest are highlighted in green, the adiabatic relaxation energies ΔE_{rlx}, obtained by subtracting the adiabatic double ionization energies corresponding to the lowest singlet states of the CH_3X^{2+} dications from their vertical counterparts (see Eq. (1) in the main text), are emphasized using blue font, and the $CH_3X^{2+} \rightarrow CHX^{2+} + H_2$ dissociation asymptotes are highlighted using magenta color. All data used to create the figure are included within it.

2.2 H_3^+ formation from organic compounds other than methyl halogens and pseudohalogens: Ethane and ethene

In this section, we report and analyze our preliminary CC and DIP-EOMCC calculations aimed at determining if our geometrical and energetic conditions (i)–(iii) laid down in the Discussion section of the main text can apply to organic compounds outside the CH_3X family. It is, for example, well-established that some hydrocarbons [3–6] and some larger alcohols [7, 8] can form H_3^+ following double ionization as well. A common feature of the species that after double ionization lead to H_3^+ formation is the presence of a neutral H_2 fragment forming a dative two-electron–three-center bond with a carbon atom in their dicationic structures, similar to the minima on the lowest singlet potentials of the H_3^+-producing CH_3X^{2+} systems obtained in our DIP-EOMCC computations discussed in the main text. Among the best examples of compounds other than those examined in our work that illustrate this feature are the doubly ionized ethanol [7, 8] and the doubly ionized ethane at an asymmetric $[CH_4–CH_2]^{2+}$ minimum on its lowest singlet potential resulting from hydrogen migration from one methyl group to another in a higher-energy $[CH_3–CH_3]^{2+}$ structure of ${C_2H_6}^{2+}$ [3, 4, 9–11]. Both ${C_2H_6}^{2+}$ minima are shown in Supplementary Figs. 5 and 6. They satisfy our geometrical conditions (i) and (ii), and if the condition (iii) is satisfied as well, the corresponding doubly ionized species are likely to produce H_3^+ in the roaming mechanism followed by proton abstraction similar to the CH_3OH^{2+}, CH_3Cl^{2+}, and CH_3NCS^{2+} dications examined in our work. This is illustrated in Supplementary Fig. 5 using the doubly ionized ethane, which produces H_3^+ [3–5], as an example. In this figure, we show the potential energy profile for the ${C_2H_6}^{2+} \rightarrow {C_2H_3}^+ + H_3^+$ reaction following double ionization of ethane, along with the ${C_2H_6}^{2+} \rightarrow {C_2H_4}^{2+} + H_2$ dissociation asymptote relevant to the roaming mechanism examined in our work, obtained in the DIP-EOMCC(3h-1p)/cc-pVDZ computations for the ${C_2H_6}^{2+}$, ${C_2H_4}^{2+}$, and ${C_2H_3}^+$ species and the CCSD/cc-pVDZ calculations for the neutral ethane, H_2, and H_3^+. In this profile, the ${C_2H_6}^{2+}$ dication, after undergoing the Jahn-Teller distortion similar to that observed in CH_3F^{2+}, CH_3Cl^{2+}, and CH_3CN^{2+}, which lifts the degeneracy of the ${}^1E_g(D_{3d})$ singlet obtained in vertical double ionization of ethane, and after relaxing to the ${}^1A_g(C_{2h})$-symmetric $[CH_3–CH_3]^{2+}$ minimum, designated in Supplementary Figs. 5 and 6 as Dication 1, in which two of the three C–H bonds at each carbon site are elongated and the distances between the associated hydrogens are close to that in H_2 (see Supplementary Table 3), undergoes hydrogen migration that leads to the formation of the $[CH_4–CH_2]^{2+}$ structure, labeled as Dication 2. In analogy to the H_3^+-producing CH_3X^{2+} systems studied in our work, the $[CH_4–CH_2]^{2+}$ species is characterized by a substantial elongation of two of the four C–H bonds at one of the two carbon atoms and the presence of a neutral H_2 fragment which subsequently roams the $[C_2H_4]^{2+}$ moiety and abstracts the proton from it to form H_3^+. This is possible since, as shown in Supplementary Fig. 5, the vertical double ionization of ethane places it above the two minima, including the key $[CH_4–CH_2]^{2+}$ (Dication 2) structure, which meets our geometrical conditions (i) and (ii), and its higher-energy $[CH_3–CH_3]^{2+}$ (Dication 1) precursor, the transition state associated with the $[CH_3–CH_3]^{2+} \rightarrow [CH_4–CH_2]^{2+}$ hydrogen migration, the dissociation asymptote corresponding to the liberation of H_2, and the final transition state connecting the $[CH_4–CH_2]^{2+}$ structure with the ${C_2H_3}^+$

and H_3^+ products. This means that all three conditions (i)–(iii) are satisfied when the ${C_2H_6}^{2+} \rightarrow {C_2H_3}^+ + H_3^+$ roaming reaction following double ionization of ethane is examined.

The situation becomes very different when the doubly ionized ethene is examined. The geometries of the neutral ethene molecule, optimized using the CCSD/cc-pVDZ approach, and of the corresponding dication in its lowest singlet state, obtained in the DIP-EOMCC(3h-1p)/cc-pVDZ calculations, are shown in Supplementary Fig. 7. The selected internuclear distances in both species, along with the vertical and adiabatic double ionization energies of ethene and the adiabatic relaxation energy characterizing its dication, $\Delta E_{\rm vert}$, $\Delta E_{\rm adiab}$, and $\Delta E_{\rm rlx}$, respectively, can be found in Supplementary Table 4. As demonstrated in Supplementary Table 4, the minimum on the lowest singlet potential energy surface of ${C_2H_4}^{2+}$, which is characterized by rotation of one of the CH_2 groups by about 86 degrees without changing the C–H distances too much, obtained by the geometrical relaxation after double ionization, violates our conditions (i) and (ii). It has been shown in Ref. [6] that hydrogen migration between the two carbon centers can take place here too, producing a more favorable structure on the lowest singlet potential energy surface that may serve as a precursor for the roaming dynamics leading to H_3^+ formation, but, according to Fig. 3 in Ref. [6], this would require overcoming high-energy barriers which are at least twice as high as the adiabatic relaxation energy $\Delta E_{\rm rlx}$ obtained in our DIP-EOMCC computations for the doubly ionized ethene reported in Supplementary Table 4. One would have to produce the ${C_2H_4}^{2+}$ dication in its high-lying excited electronic states located above these barriers and undergo nonadiabatic transitions to the lowest-energy singlet potential of ${C_2H_4}^{2+}$ in order for H_3^+ to form. This explains the very low yield of H_3^+ from the doubly ionized ethene observed experimentally [5, 6] and is consistent with the fact that the ${C_2H_4}^{2+}$ dication violates our conditions (i)–(iii).

The above considerations show that it is likely that the three conditions laid down in the Discussion section are applicable to organic compounds of astrophysical significance outside the CH_3X family, such as hydrocarbons and larger alcohols, but additional factors may have to be considered as well. As implied by the above analysis of ethane, for example, doubly ionized hydrocarbons may require an additional migration of hydrogen between carbon sites to create structures having elongated C–H bonds and H–H distance close to the isolated H_2 that can serve as precursors to the roaming mechanism considered in our study. In the case of larger alcohols, we should keep in mind that the doubly ionized longer-chain saturated alcohol molecules examined in Ref. [7] show a decrease in the H_3^+ yield due to an increase in the number of other competing fragmentation and energy-relaxation pathways. All of this means that this topic needs more study, but it is certainly interesting to observe that our conditions (i)–(iii), developed in the context of examining H_3^+ formation from the doubly ionized methyl halides and pseudohalides, apply to at least some organic compounds outside the CH_3X family.

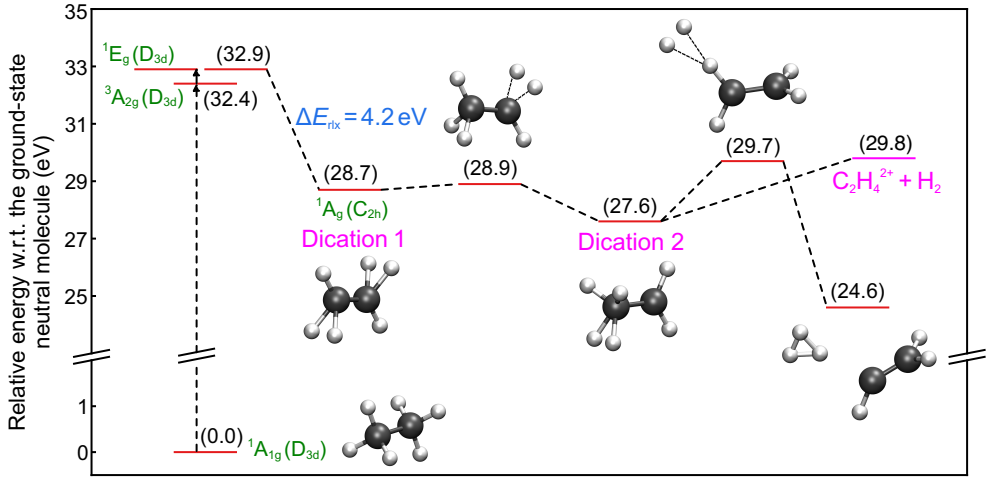

Supplementary Fig. 5: Potential energy profile for H_3^+ formation from doubly ionized ethane. The energy profile (in eV) illustrates the $C_2H_6^{2+} \rightarrow C_2H_3^+ + H_3^+$ reaction following double ionization of ethane, along with the $C_2H_6^{2+} \rightarrow C_2H_4^{2+} + H_2$ dissociation asymptote relevant to the roaming mechanism examined in the present study, obtained in the DIP-EOMCC(3h-1p)/cc-pVDZ computations for the $C_2H_6^{2+}$, $C_2H_4^{2+}$, and $C_2H_3^+$ species and the CCSD/cc-pVDZ calculations for the neutral ethane, H_2, and H_3^+. The $C_2H_6^{2+}$ dication, after undergoing the Jahn-Teller distortion that lifts the degeneracy of the $^1E_g(D_{3d})$ singlet state resulting from vertical double ionization of ethane, and after relaxing to the $^1A_g(C_{2h})$-symmetric $[CH_3–CH_3]^{2+}$ minimum, designated as Dication 1, undergoes hydrogen migration that leads to the formation of the lower-energy $[CH_4–CH_2]^{2+}$ structure, labeled as Dication 2. The asymmetric $[CH_4–CH_2]^{2+}$ species is characterized by a substantial elongation of two of the four C–H bonds at one of its carbon centers and the presence of a neutral H_2 fragment, which subsequently roams the $[C_2H_4]^{2+}$ moiety and abstracts the proton from it to form H_3^+. The multiplicities, irreducible representations, and point group symmetries of the low-lying electronic states of the $C_2H_6^{2+}$ dication are highlighted in green and the adiabatic relaxation energy $\Delta E_{\rm rlx}$, obtained by subtracting the energy of the $^1A_g(C_{2h})$-symmetric $[CH_3–CH_3]^{2+}$ structure from the energy of the $^1E_g(D_{3d})$ state resulting from vertical double ionization of ethane (see Eq. (1) in the main text), is emphasized using blue font. The $C_2H_6^{2+} \rightarrow C_2H_4^{2+} + H_2$ dissociation asymptote and the $[CH_3–CH_3]^{2+}$ (Dication 1) and $[CH_4–CH_2]^{2+}$ (Dication 2) minima are highlighted using magenta color. All data used to create the figure are included within it.

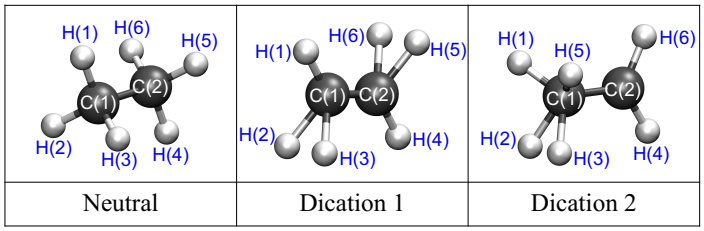

Neutral	Dication 1	Dication 2

Supplementary Fig. 6: Molecular structures of ethane and its dications. Shown are the geometries of ethane and the $[CH_3–CH_3]^{2+}$ and $[CH_4–CH_2]^{2+}$ minima on the lowest singlet potential energy surface of the ${C_2H_6}^{2+}$ species, designated in Supplementary Fig. 5 as Dication 1 and Dication 2, respectively, resulting from the CCSD (ethane) and DIP-EOMCC(3h-1p) ($[CH_3–CH_3]^{2+}$ and $[CH_4–CH_2]^{2+}$) geometry optimizations using the cc-pVDZ basis set. The $^1A_g(C_{2h})$-symmetric Dication 1 is a local minimum into which ${C_2H_6}^{2+}$ relaxes following double ionization of ethane. The lower-energy Dication 2 structure emerges when one of the hydrogen atoms, designated in the figure as H(5), migrates from one methyl group in Dication 1 to another. The corresponding C–H and H–H bond lengths are given in Supplementary Table 3.

Supplementary Table 3: Comparison of the selected internuclear distances, in Å, characterizing the $[CH_3–CH_3]^{2+}$ and $[CH_4–CH_2]^{2+}$ structures on the lowest singlet potential of ${C_2H_6}^{2+}$, designated in Supplementary Figs. 5 and 6 as Dication 1 and Dication 2, respectively, which are most relevant to H_3^+ formation, with their counterparts in the neutral ethane molecule. The equilibrium geometry of ethane was optimized using the CCSD/cc-pVDZ approach, whereas those of the Dication 1 and Dication 2 structures were obtained with DIP-EOMCC(3h-1p)/cc-pVDZ.

	Bond length		
Bond	Neutral	Dication 1	Dication 2
C(1)–H(1)	1.105	1.103	1.137
C(1)–H(2)	1.105	1.248	1.231
C(1)–H(3)	1.105	1.248	1.231
C(1)–H(5)	2.191	2.168	1.137
C(2)–H(4)	1.105	1.103	1.108
C(2)–H(5)	1.105	1.248	2.200
C(2)–H(6)	1.105	1.248	1.108
H(1)–H(5)	2.551	2.606	1.694
H(2)–H(3)	1.784	0.987	0.969
H(5)–H(6)	1.784	0.987	2.637

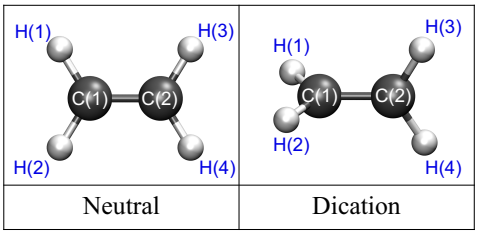

Supplementary Fig. 7: Molecular structures of ethene and its dication. Shown are the geometries of the neutral ethene molecule, optimized using the CCSD/cc-pVDZ approach, and of the corresponding $C_2H_4^{2+}$ dication in its lowest singlet state, obtained in the DIP-EOMCC(3h-1p)/cc-pVDZ calculations. The corresponding C–H and H–H bond lengths are given in Supplementary Table 4.

Supplementary Table 4: Comparison of the selected internuclear distances, in Å, characterizing the doubly ionized ethene molecule in its lowest singlet state with their counterparts in the neutral C_2H_4 species, along with the corresponding vertical and adiabatic double ionization energies, $\Delta E_{\rm vert}$ and $\Delta E_{\rm adiab}$, respectively, and the adiabatic relaxation energy $\Delta E_{\rm rlx}$ associated with the $C_2H_4^{2+}$ dication shown in Supplementary Fig. 7, in eV (for the definition of $\Delta E_{\rm rlx}$, see Eq. (1) in the main text). The equilibrium geometry and energetics of ethene were computed with the CCSD/cc-pVDZ approach, whereas the structural parameters of the $C_2H_4^{2+}$ species in its lowest singlet state and the associated $\Delta E_{\rm vert}$, $\Delta E_{\rm adiab}$, and $\Delta E_{\rm rlx}$ values were determined using DIP-EOMCC(3h-1p)/cc-pVDZ.

Bond length				
Bond	Neutral	Dication	Energy type	
C(1)–H(1)	1.097	1.132	$\Delta E_{\rm vert}$	30.6
C(1)–H(2)	1.097	1.132	$\Delta E_{\rm adiab}$	28.0
C(2)–H(3)	1.097	1.132	$\Delta E_{\rm rlx}$	2.6
C(2)–H(4)	1.097	1.132		
H(1)–H(2)	1.870	1.945		
H(3)–H(4)	1.870	1.946		

References

[1] Matsubara, T.: Dynamic effects on the ionization-induced reactions of methyl halides: Quantum mechanical and molecular dynamics studies. J. Phys. Chem. A **127**, 4801–4814 (2023)

[2] Ando, T., Shimamoto, A., Miura, S., Iwasaki, A., Nakai, K., Yamanouchi, K.: Coherent vibrations in methanol cation probed by periodic H_3^+ ejection after double ionization. Commun. Chem. **1**, 7 (2018)

[3] Zhang, Y., Ren, B., Yang, C.-L., Wei, L., Wang, B., Han, J., Yu, W., Qi, Y., Zou, Y., Chen, L., Wang, E., Wei, B.: Formation of H_3^+ from ethane dication induced by electron impact. Commun. Chem. **3**, 160 (2020)

[4] Hoshina, K., Kawamura, H., Tsuge, M., Tamiya, M., Ishiguro, M.: Metastable decomposition and hydrogen migration of ethane dication produced in an intense femtosecond near-infrared laser field. J. Chem. Phys. **134**, 064324 (2011)

[5] Hoshina, K., Furukawa, Y., Okino, T., Yamanouchi, K.: Efficient ejection of H_3^+ from hydrocarbon molecules induced by ultrashort intense laser fields. J. Chem. Phys. **129**, 104302 (2008)

[6] Zhang, Y., Wei, L., Yang, C.-L., Yu, W., Wang, B., Yan, B., Zou, Y., Chen, L., Wei, B.: Formation of H_3^+ from hydrocarbon dications induced by collisions with charged particles. Phys. Rev. A **100**, 052706 (2019)

[7] Ekanayake, N., Severt, T., Nairat, M., Weingartz, N.P., Farris, B.M., Kaderiya, B., Feizollah, P., Jochim, B., Ziaee, F., Borne, K., P., K.R., Carnes, K.D., Rolles, D., Rudenko, A., Levine, B.G., Jackson, J.E., Ben-Itzhak, I., Dantus, M.: H_2 roaming chemistry and the formation of $H_3{}^+$ from organic molecules in strong laser fields. Nat. Commun. **9**, 5186 (2018)

[8] Severt, T., Weckwerth, E., Kaderiya, B., Feizollah, P., Jochim, B., Borne, K., Ziaee, F., Pandiri, K.R., Carnes, K.D., Dantus, M., Rolles, D., Rudenko, A., Wells, E., Ben-Itzhak, I.: Initial-site characterization of hydrogen migration following strong-field double-ionization of ethanol. Nat. Commun. **15**, 74 (2024)

[9] Lammertsma, K., Olah, G.A., Barzaghi, M., Simonetta, M.: Diprotonated methane, CH_6^{2+}, and diprotonated ethane, $C_2H_8^{2+}$. J. Am. Chem. Soc. **104**, 6851–6852 (1982)

[10] Rasul, G., Prakash, G.K.S., Olah, G.A.: Comparative ab initio study of the structures and stabilities of the ethane dication $C_2H_6^{2+}$ and its silicon analogues $Si_2H_6^{2+}$ and $CSiH_6^{2+}$. J. Phys. Chem. A **109**, 798–801 (2005)

[11] Wei, L., Lam, C.-S., Zhang, Y., Ren, B., Han, J., Wang, B., Zou, Y., Chen, L., Lau, K.-C., Wei, B.: Isomerization dynamics in the symmetric and asymmetric

fragmentation of ethane dications. J. Phys. Chem. Lett. **12**, 5789–5795 (2021)